Chapter 1
X-57 Mod III Wing Ground Vibration Test

Truong Samson, Bhamidipati Keerti, Lung Shun-Fat, Spivey Natalie, Truax Roger, and Winkel James

Abstract The X-57 "Maxwell" all-electric experimental aircraft was an electric propulsion demonstrator developed by the National Aeronautics and Space Administration to inform airworthiness standards for electrified aircraft. The development of the X-57 aircraft was separated into configuration modifications culminating in a distributed electric propulsion flight demonstrator named Modification IV (a.k.a., Mod IV). One of these configurations, the X-57 Mod III aircraft, involved flight-testing of a long, slender, high-aspect-ratio wing with two electric motors located at the wingtips. The X-57 Mod III wing ground vibration test was performed in the Flight Loads Laboratory at the National Aeronautics and Space Administration Armstrong Flight Research Center to measure the structural dynamics properties of the newly developed wing, and to confirm airworthiness of the Mod III/IV aircraft. This paper describes the testing performed to acquire the modal data and the subsequent results from the test.

Keywords Electric · Ground Vibration Test · Modal · X-57

Introduction

The X-57 "Maxwell" all-electric experimental aircraft was based on a modified general aviation Tecnam P2006T (TECNAM S.p.A., Costruzioni Aeronautiche Tecnam, Capua, Italy) twin engine airplane [1, 2]. The plan was to have the X-57 aircraft undergo several iterative modifications, building up to a distributed-electric propulsion demonstrator aircraft. The originally planned modification sequence is shown in Fig. 1. Midway through the project lifecycle, the third and fourth modifications were merged as Modification (Mod III/IV). Modification (Mod) I is the baseline Tecnam P2006T airplane with two inboard gas-powered engines. Mod II expanded on Mod I by replacing the gas-powered engines with electric motors that were powered by traction batteries. The plan for Mod III/ IV was to incorporate a new high-aspect-ratio wing design with the two electric cruise motors moved outboard to the wingtips as well as 12 high-lift electric motors mounted and distributed along the wing leading edge. The X-57 project, however, was cancelled before Mod III/IV took flight.

The National Aeronautics and Space Administration (NASA) Armstrong Flight Research Center (AFRC) Flight Loads Laboratory (FLL) [3–5] conducted a ground vibration test (GVT) on the X-57 Mod III wing, as shown in Fig. 2, in order to gather the wing modal data to correlate to the fundamental wing modes in the finite element model (FEM). The resulting tuned FEM helped with early updates to the classical and whirl flutter analyses for the Mod III and Mod IV aircraft. Also, having the GVT performed early in the wing design process helped reduced programmatic risk by identifying any problems before the wing was mounted to the aircraft fuselage. Two main configurations were tested, one was the Mod III wing with the cruise motor nacelle mass simulators at the wingtips, as shown in Fig. 2, and the other was the clean wing on its own, as shown in Fig. 3. The Mod III wing GVT was conducted prior to the fabrication of wingtip cruise motor nacelles; therefore, cruise motor nacelle mass simulators were used. The Mod III wing was mounted on the wing loads test fixture (WLTF) as the GVT was conducted using a text fixture shared with the wing proof loads test [6]. The test also incorporated various flap and aileron settings to measure the effect of deployment on the control surface modes. A total of 192 test runs were performed for the X-57 Mod III wing GVT from May to June 2019.

Truong Samson · Bhamidipati Keerti · Lung Shun-Fat · Spivey Natalie · Truax Roger
NASA Armstrong Flight Research Center, Armstrong Flight Research Center, 4800 Lilly Avenue, Edwards, CA, 93523 USA
e-mail: samson.s.truong@nasa.gov; keerti.k.bhamidipati@nasa.gov; shun-fat.lung-1@nasa.gov; natalie.d.spivey@nasa.gov; dutrieux42@gmail.com

Winkel James
NASA Langley Research Center, Langley Research Center, 1 Nasa Dr, Hampton, VA, 23666 USA
e-mail: james.winkel@nasa.gov

Chad Walber et al. (eds.), *Sensors & Instrumentation and Aircraft/Aerospace Testing Techniques, Vol. 8*, Conference Proceedings of the Society for Experimental Mechanics Series, https://doi.org/10.13052/97887-438-0153-5_1

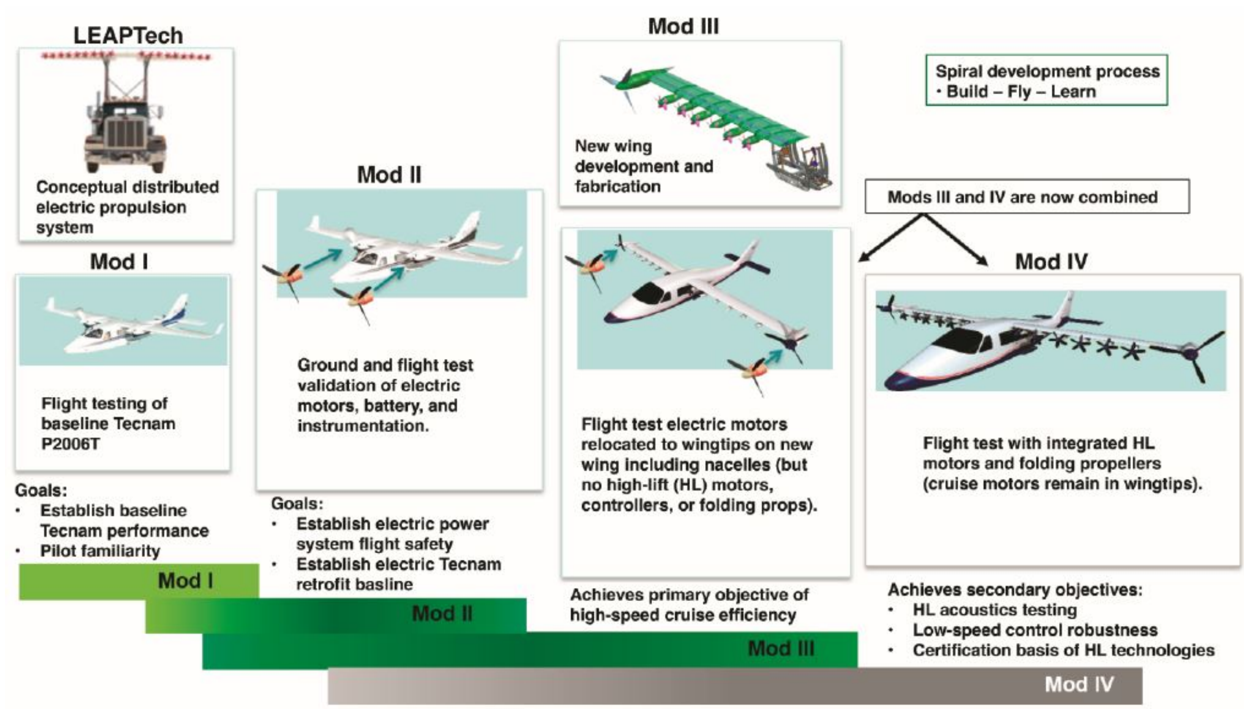

Fig. 1 X-57 Maxwell configuration modifications

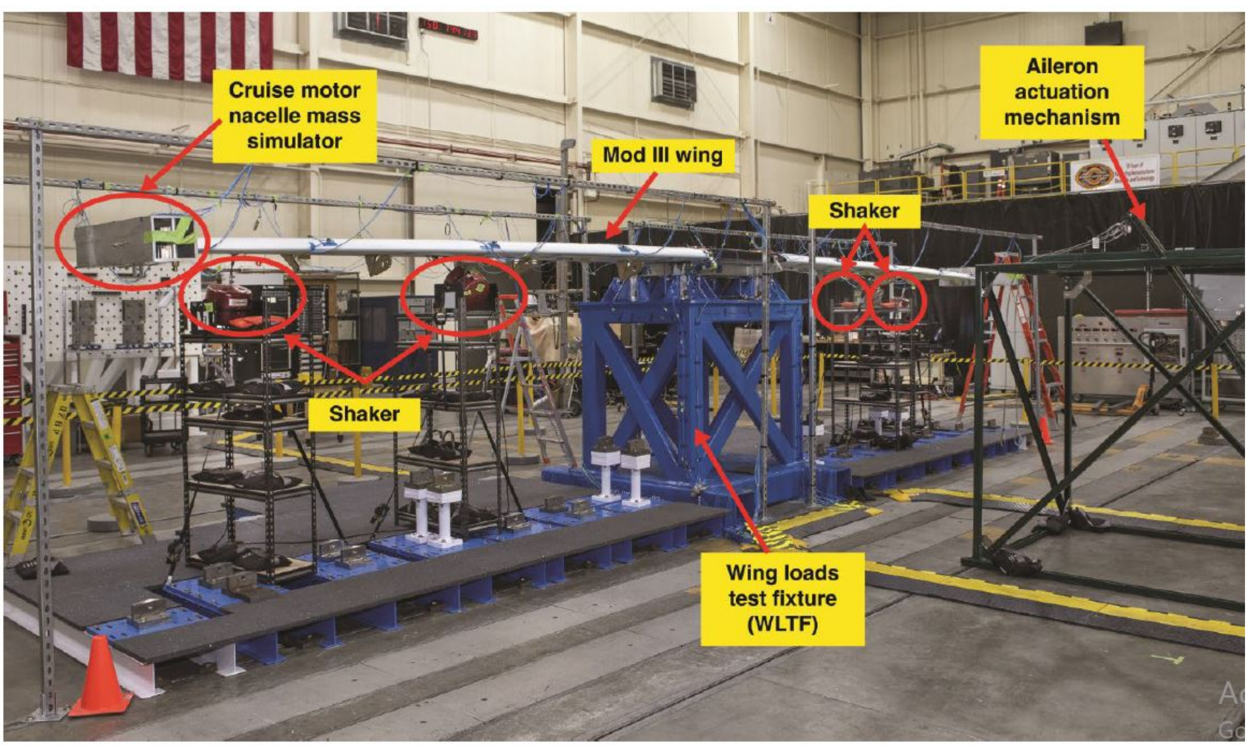

Fig. 2 X-57 Mod III wing ground vibration test setup in the Flight Loads Laboratory at Armstrong Flight Research Center. Setup shown in a four-shaker configuration

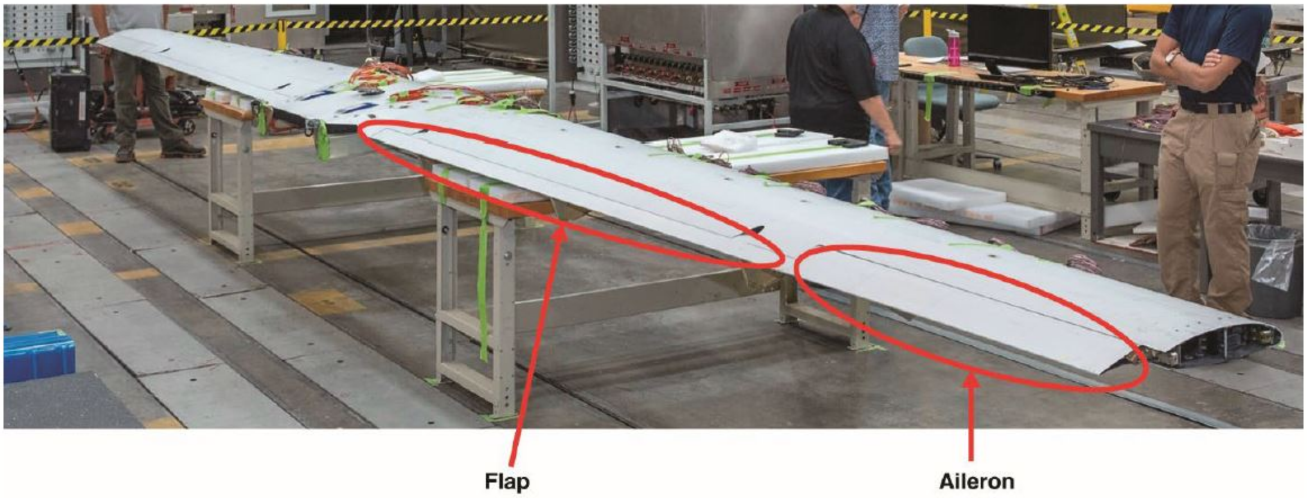

Fig. 3 X-57 Mod III clean wing at the National Aeronautics and Space Administration Armstrong Flight Research Center Flight Loads Laboratory

Test Objectives

The objective of the GVT was to capture modes that were predicted to be participants in the wing flutter mechanism [7]. For the primary objectives, frequencies, mode shapes, and damping were collected for wing 1st bending (W1B); wing 2nd bending (W2B); wing 1st torsion (W1T), wing fore/aft; and bending and rotation modes of the flaps and ailerons (early FEM predictions indicated significant responses from the control surfaces). Secondary objectives included measuring control surface modes for the clean wing configuration to understand the effect of wing deflection (resulting from the wingtip mounted motors) on the control surface modes. Data gathered during the GVT helped characterize the Mod III wing structure and facilitate updates to the wing FEM model. The tuned FEM was used to update both the classical and whirl flutter analyses after the GVT.

Test Description

The following sections go further into detail about the X-57 Mod III wing test article, the finite element model, and additional details of the GVT.

Test Article

The original Tecnam P2006T wing was to be replaced with a newly constructed wing for the X-57 Mod III/IV aircraft. The Mod III/IV wing was manufactured by Empirical Systems Aerospace, Inc. (ESAero) (San Luis Obispo, California). Unlike the original P2006T, the Mod III wing was designed to have a smaller chord and a higher-aspect-ratio wing when compared to the original P2006T wing, which would help increase cruise flight efficiency. Table 1 shows the various dimensions and weight specifications for the Mod III wing. Note that the weights in this table were provided in April 2019, which was prior to the X-57 Mod III wing GVT.

For this GVT, two different configurations were tested:

- Configuration A: wing + wingtip mounting plates + cruise nacelle mass simulators
- Configuration B: clean wing

Configuration A was tested first, and since the wingtip cruise nacelles and electric motors had not yet been fabricated at the time, mass simulators were added at the ends of each wingtip to simulate the actual mass and center-of-gravity locations of the real electric cruise motors. For these mass simulators to interface with the wing, wingtip plates had to be made and were installed at the end of each wing, which then allowed the mass simulators to be mounted onto the wing plates. After the GVT of configuration A was completed, the cruise nacelle mass simulators as well as the wingtip plates were removed

Table 1 X-57 Mod III wing specifications (as of April 2019) prior to the ground vibration test

Wing properties	Dimensions
Aspect ratio	15
Mean aerodynamic chord	2.13 ft
Wingspan	31.63 ft
Wing area	67 ft^2
Taper ratio	0.7
Tip chord	1.74 ft
Root chord	2.48 ft
Weight (clean wing including H-frame)	313.5 lb
Weight (wing + wingtip mounting plates)	352.5 lb
Weight (wing + wingtip mounting plates + cruise nacelle mass simulators ($\times$ 2))	581.5 lb
Mod III estimate for weight (cruise nacelle ($\times$1))	134 lb

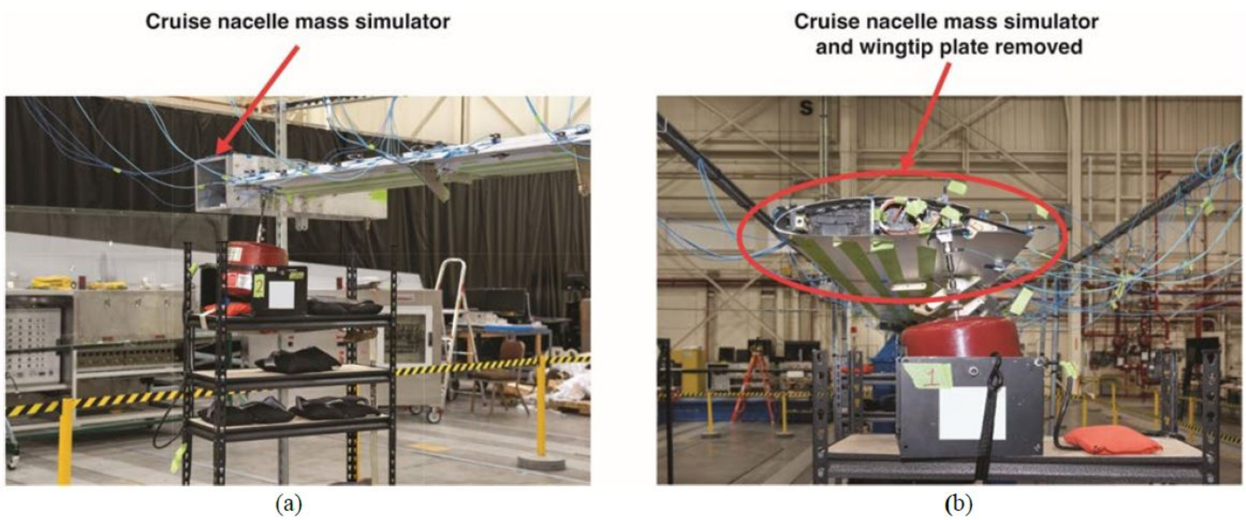

Fig. 4 X-57 Mod III wing ground vibration test configuration A (Fig. 4a); and configuration B (Fig. 4b)

for configuration B for the clean Mod III wing. Figure 4 shows the differences between the two GVT configurations at the wingtips (Fig. 4a and Fig. 4b).

Finite Element Model

The X-57 Mod III wing FEM was used for both modal and flutter analysis to generate pre-test predictions for the GVT. The FEM modal analysis was performed using MSC Nastran (MSC Software Corporation, Newport Beach, California) for the Mod III wing for boundary conditions of the wing fixed at the H-frame mounting points, as well as the wing mounted on the WLTF. Figure 5 shows the FEM models for configuration A (Fig. 5a) with the cruise nacelles, and configuration B (Fig. 5b) with only the clean wing.

For the fixed-wing boundary case, the four attachment points of the H-frame underneath the Mod III wing, which connect the wing to the fuselage, were rigidly fixed in all degrees of freedom (DOF). Figure 6 shows the location of the H-frame with respect to the Mod III wing.

In addition to the fixed-wing FEM predictions, modal analysis was performed with the Mod III wing FEM on the WLTF FEM for comparison between the two, as shown in Fig. 7. The WLTF was designed and fabricated by Pyramid Space, Inc. (Carlsbad, California) and allowed the Mod III wing to be mounted on the fixture in the FLL for both the GVT as well as the proof loads test.

The WLTF has eight bolt locations (two at each corner) so that it can be bolted into the floor tracks of the FLL. Initially, the WLTF FEM had all eight bolt locations rigidly fixed, resulting in a FEM prediction of 72.08 Hz for its 1st frequency.

Fig. 5 X-57 Mod III wing finite element model configuration A (Fig. 5a) with the cruise nacelles; and configuration B (Fig. 5b) with only the clean wing.

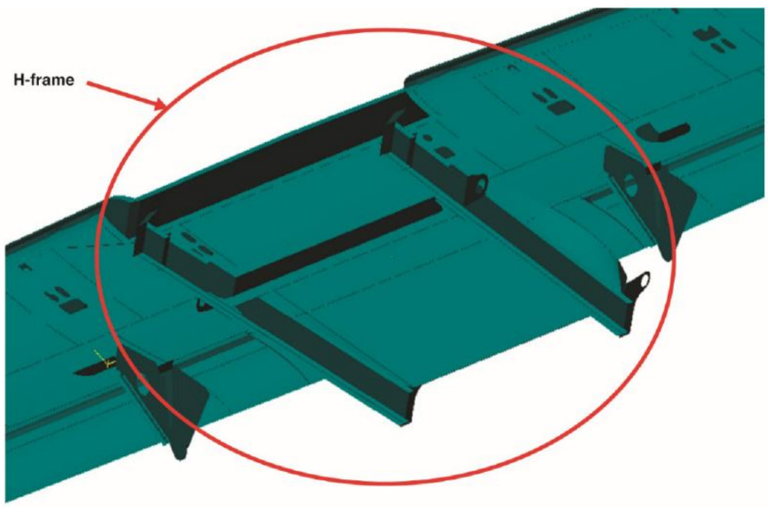

Fig. 6 H-frame location underneath the X-57 Mod III wing

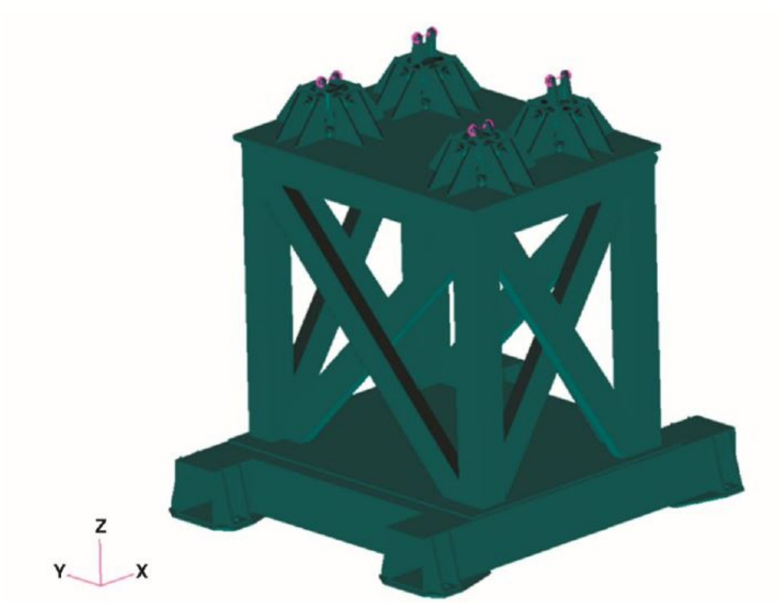

Fig. 7 Finite element model for the wing loads test fixture

For the FEM prediction verification, a small GVT was performed with the WLTF in the FLL prior to the X-57 Mod III Wing GVT. It was found that the 1st frequency of the WLTF was 58.38 Hz, about 23 percent lower than what was initially predicted. To model the boundary condition more closely to what was observed, the WLTF FEM was updated with each of the bolt locations having both X- and Y-axes rigidly fixed as a Rigid Body Element type 3 point, while the Z-axis translational vertical direction was fixed via a stiff CELAS2 spring, as shown in Fig. 8. The updated WLTF FEM boundary condition resulted in a 1st frequency of 55.68 Hz, which was close to what was seen in the WLTF GVT.

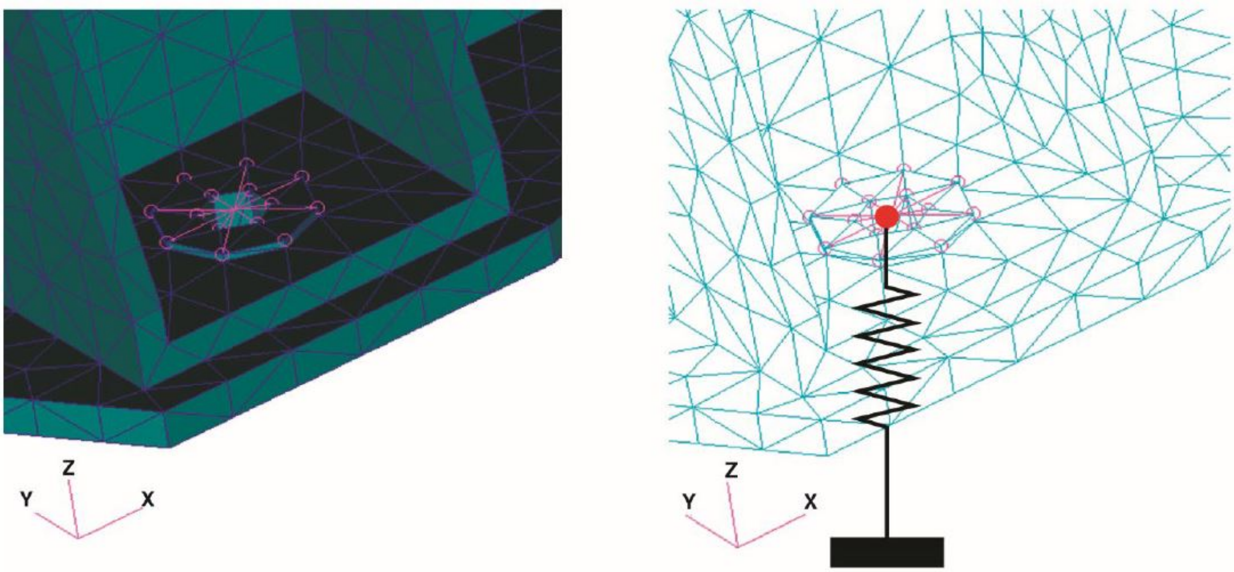

Fig. 8 Updated wing loads test fixture finite element model boundary condition, with the center of the Rigid Body Element type 3 point fixed in the Z-axis translational vertical direction via a stiff CELAS2 spring

The WLTF FEM with the updated boundary condition was then mated with both Mod III wing configurations, as shown in Fig. 9. The resulting FEM modal frequencies between the fixed-wing-only case and the wing with the WLTF were very similar for both configuration A (Fig. 9a) and configuration B (Fig. 9b). It should be noted that for both configurations, coupling was seen in the mode shapes between the Mod III wing and the WLTF at around 52 Hz.

Fig. 9 Finite element model for the X-57 Mod III wing on the wing loads test fixture for configuration A (Fig.9a); and configuration B (Fig.9b).

Test Configurations

Table 2 shows an example of the test configuration matrix used by the NASA AFRC structural dynamic test engineers to ensure that the test objectives were achieved. The table highlights the different test cases with varying aileron or flap position and excitation methods, locations, or directions. At the discretion of the test engineers, test cases B2 and B6 were

Table 2 Test configuration matrix for the X-57 Mod III wing ground vibration test

Configuration		Test case	Aileron position	Flap position	Shaker / impact	Shaker/impact locations	Shaker/ impact direction	Shaker force level
Configuration A	Wing with cruise nacelle simulators	A1	Locked & neutral	Locked & stowed (0%)	Shaker (x2)	Wing TE spar	30° F/A, Vert, F/A, lat	Low, med, high
		A2			Shaker (x4)	Wing TE spar & flap TE center		
		A3			Shaker / impact	Control surfaces OB TE & TE center	Vert, F/A	Low
		A4	Unlocked & neutral		Shaker (x2)	Wing TE spar	30° F/A, Vert, F/A, lat	Low, med, high
		A5			Shaker / impact	Control surfaces OB TE & TE center	Vert, F/A	Low
		A6	Locked & neutral	Locked & slightly deployed (0% - just off stops)			Vert, lat, F/A	
		A7		Locked & deployed (100% - relevel accels)				
Configuration B	Clean wing	B1	Locked & neutral	Locked & stowed (0%)	Shaker (x2)	Wing TE spar	30° F/A, vert, F/A, lat	Low, med, high
		B2			Shaker (x4)	Wing TE spar & flap TE center		
		B3			Shaker / impact	Control surfaces OB TE & TE center	Vert, F/A	Low
		B4	Unlocked & neutral		Shaker (x2)	Wing TE spar	30° F/A, vert, F/A, lat	Low, med, high
		B5			Shaker / impact	Control surfaces OB TE & TE center	Vert, F/A	Low
		B6	Locked & neutral	Locked & slightly deployed (0% - just off stops)			Vert, lat, F/A	
		B7		Locked & deployed (100% - relevel accels)				

Accelerometer (accel); fore/aft (F/A); lateral (lat); outboard (OB); trailing edge (TE); vertical (vert)

not performed. For test case B2, it was found that a four-shaker setup in configuration A did not yield clean data as desired. Test case B6 was a secondary objective and was eliminated due to time constraints.

Ailerons were never deflected during the GVT and were either locked or unlocked at a neutral setting. Figure 10 shows an aileron actuation mechanism device, shown as the green Unistrut frame (Fig. 10a), and a close-up view that was constructed in front of the Mod III wing leading edge to lock the ailerons manually (Fig. 10b). Two cables were connected to the left and right ailerons, and each cable required about 44 lb of force to lock the ailerons in place. In-line load cells were placed on these cables to monitor the loads during the test. For any test cases that involved unlocked ailerons, the cables were disconnected and removed.

(a) (b)

Fig. 10 Aileron actuation mechanism in front of the X-57 Mod III wing (Fig. 10a); and close-up view with the cables attached (Fig. 10b)

The Mod III wing flaps were driven by an actuator that locked the flap position when unpowered in all test cases. Flap position settings used during the GVT were stowed, slightly deployed (released just off their stops), and fully deployed at the maximum setting. It should be noted that the stowed and slightly deployed flap configurations were considered a 0-deg flap deflection setting, while the fully deployed flap case was considered a 30-deg flap deflection setting. For test cases that required the flaps to be slightly deployed or fully deployed, an external power supply was connected to electrically actuate the flaps to the desired position prior to test execution. Cables connecting the flap to the external power supply were disconnected before performing the test runs to avoid unwanted mass to the test article. Furthermore, for the fully deployed flap setting, GVT accelerometers on the flaps had to be releveled as their orientations had changed. Excitation was predominantly done with two shakers, one at each of the wingtips, oriented either vertically or fore/aft depending on the test run. There were several test runs that had a four-shaker configuration, as shown in Fig. 2, with an additional shaker located at each of the left and right flaps. An impact hammer excitation was also used, primarily for the control surface investigation.

Ground Vibration Test Setup

Prior to the GVT, both weight and balance measurements were performed on the X-57 Mod III wing. Due to the flap actuator mechanism located near the left outboard wingtip, about 5 lb of ballast had to be placed on the right-wing side to keep the wing level. This additional weight was considered for subsequent updated weight and center-of-gravity calculations. Before installing the Mod III wing onto the WLTF, the test fixture itself was torqued to 220lb ($\pm$20 ft-lb) to the FLL floor tracks and shimmed to provide leveling. For configuration A, the wingtip plates and cruise nacelle mass simulators were installed onto the Mod III wingtips before the wing was mounted onto the WLTF. These wingtip plates and cruise nacelle mass simulators were later removed for configuration B for the clean wing case. At the time of the X-57 Mod III wing GVT, the flight accelerometers for the wing were not ready, so no data was collected during the GVT using flight instrumentation.

Ground Vibration Test Instrumentation

For the X-57 Mod III wing GVT, the data acquisition (DAQ) used was the LAN-XI DAQ hardware system (Brüel & Kjær, Nærum, Denmark), which was the first large-scale GVT by NASA AFRC using this DAQ system. Four mainframes were used, including two LAN-XI Type 3660-D11-slot mainframes and two LAN-XI Type 3660-C 5-slot mainframes, and were all connected via a network switch. Accelerometer outputs and force transducers for both the impact hammer and shakers were connected to the 12-channel accelerometer LAN-XI Type 3053 modules and shaker generator LAN-XI Type 3160 modules. The setup of the LAN-XI DAQ hardware is shown in Fig. 11.

Two different types of accelerometer sensors were used for this test, including the PCB T356A16 low-frequency triaxial and the PCB T33B32 low-frequency uniaxial (PCB Piezoelectronics, Inc., Depew, New York). The Mod III wing and its flaps and ailerons, as well as portions of the H-frame and the wingtip plates (used to interface the cruise nacelle mass simulator to the wing) were instrumented with these PCB T356A16 triaxial accelerometers. The WLTF, the cruise nacelle mass simulators, and the connection points between the WLTF and the H-frame were instrumented with PCB T33B32

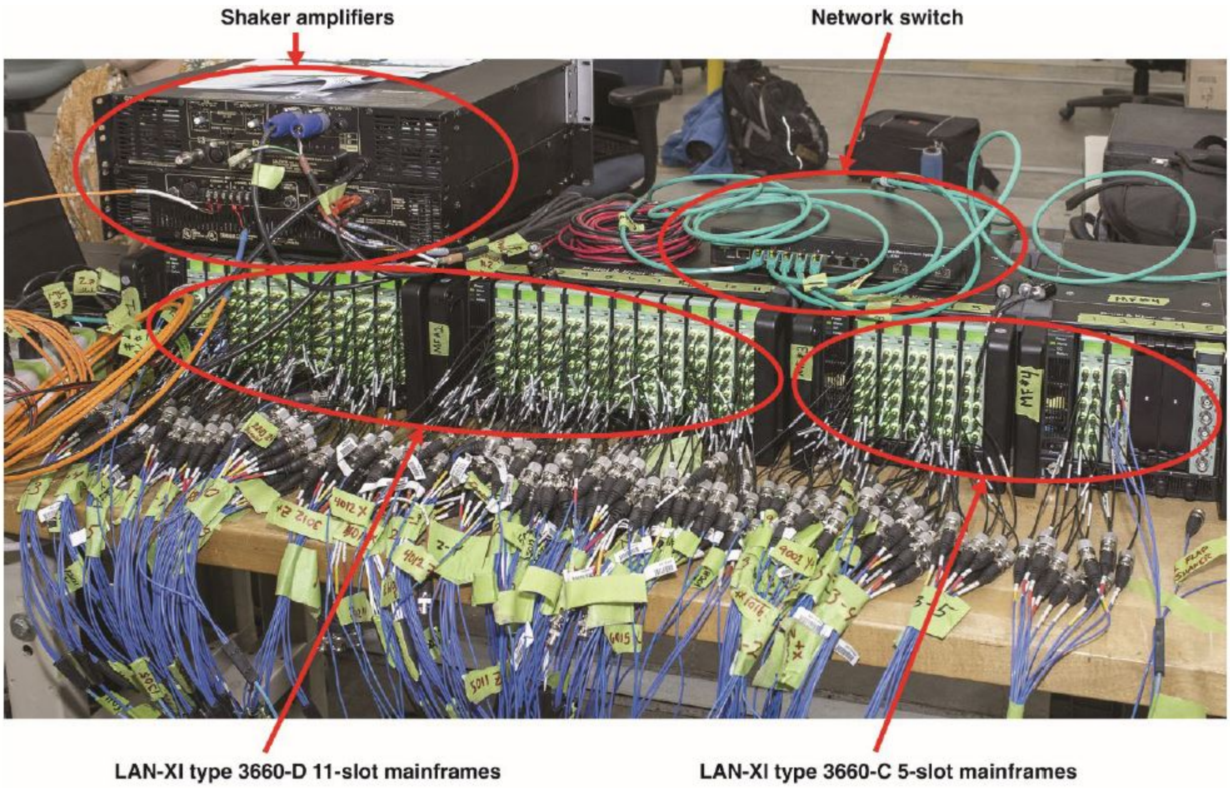

Fig. 11 LAN-XI data acquisition hardware system used for the X-57 Mod III wing ground vibration test

uniaxial accelerometers. It should be noted that for this GVT, data was gathered in all three degrees of freedom for all test node locations. At some test node locations, three uniaxial accelerometers were used to build up a triaxial measurement.

The excitation for this GVT was provided using both shakers and an impact hammer. The shakers were used to excite throughout the wing structure, while the impact hammer was used for local excitation of the individual control surfaces. Two different MB Dynamics (MB Dynamics, Inc., Cleveland, Ohio) electromagnetic shaker types were used, the Modal 110 and the Modal 50A. Depending on the test case for a particular run, either a two-shaker or a four-shaker configuration was u

Ground Vibration Test Accelerometer Layout

For configuration A of the X-57 Mod III wing GVT, a total of 104 accelerometer locations were installed measuring 312 DOF, whereas for configuration B with the clean wing (i.e., cruise nacelle mass simulators and wingtip plates removed), there were 96 total accelerometer locations measuring 288 DOF. Accelerometers were installed at various locations for the X-57 Mod III wing along the spars and ribs of the wing and along the hinge lines for the control surfaces. All sensors were installed using the global coordinate system of the airplane. It should be noted that several of the flap leading edge accelerometers had to be installed on the underside of the wing to avoid interference with the wing in the stowed-flaps configuration. Table 3 shows the number of accelerometers and DOF count for this GVT.

Table 3 Accelerometer and degrees of freedom count breakdown for the X-57 Mod III wing ground vibration test

Description	# of accelerometer locations	# of DOF
Wing	81	243
H-frame	7	21
Wing loads test fixture (WLTF)	8	24
Cruise nacelle mass simulators and wingtip plates	8	24
Total	104	312

The numbering convention for all the various accelerometer locations of this GVT is detailed in Table 4. The triaxial accelerometer locations for the wing are shown in Fig. 12.

Table 4 X-57 Mod III wing ground vibration test accelerometer node numbering convention

Description	Node Series #	Description	Node Series #
Left wing forward spar	1100	Right aileron	6000
Left wing mid spar	1200	Wing center	7000
Left wing aft spar	1300	Left cruise nacelle simulator	8100
Right wing forward spar	2100	Right cruise nacelle simulator	8200
Right wing mid spar	2200	Left mass simulator plate	8300
Right wing aft spar	2300	Right mass simulator plate	8400
Left flap	3000	Wing loads test fixture (WLTF)	9000
Right flap	4000	WLTF attachment points	9100
Left aileron	5000	H-frame	9200

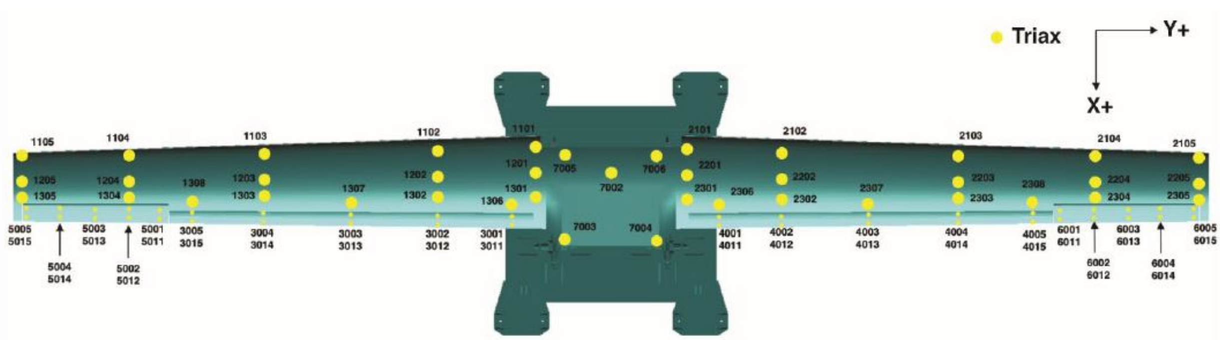

Fig. 12 Ground vibration test triaxial accelerometer locations for the X-57 Mod III wing

Figure 13 shows the triaxial accelerometer locations for the H-frame. Notice that the forward WLTF connection points to the H-frame do not line up linearly underneath, exactly where the forward wing points attach to the H-frame.

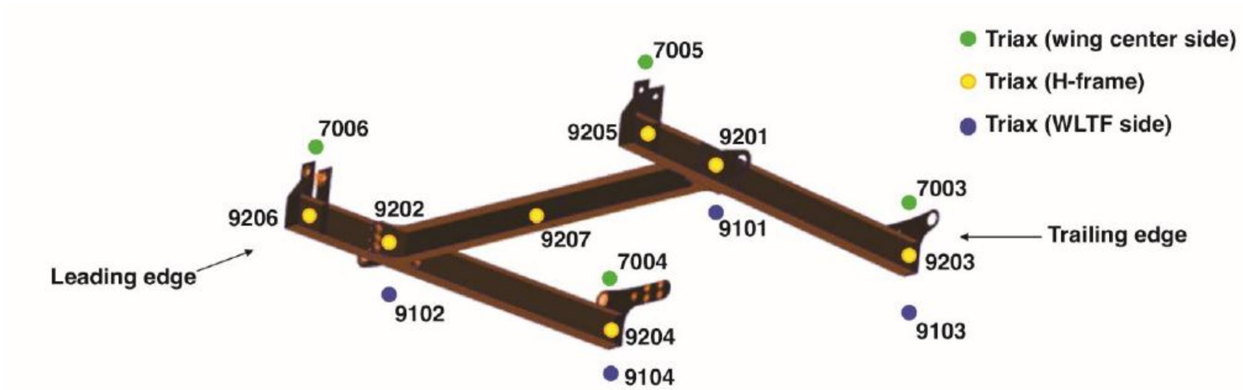

Fig. 13 Ground vibration test triaxial accelerometer locations for the H-frame, with other accelerometers on the wing and the wing loads test fixture side for reference

Figure 14 shows the triaxial accelerometer locations for the WLTF during the test. Since the GVT had been previously performed on the WLTF by itself and, at the time, confirmed that its 1st frequency was above most of the modal frequencies of interest for the Mod III wing, only the top portions of the WLTF and its connection points to the wing, via the H-frame adapter, were instrumented with accelerometers. For the cruise nacelle mass simulators and the wingtip plates, there were only eight total accelerometer locations, with one sensor each, located at both the forward and aft ends.

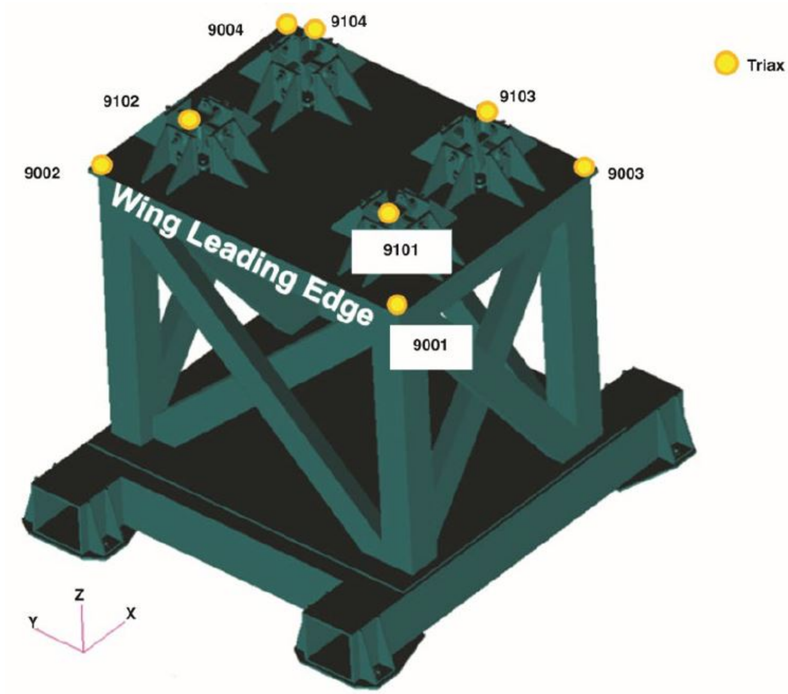

Fig. 14 Ground vibration test triaxial accelerometer locations for the wing loads test fixture

Test Display Model

The GVT test display models were created in the BK Connect® (Brüel & Kjær, Nærum, Denmark) software with triangular elements and assisted the test engineers with visualizing the test mode shapes throughout testing. Due to the large deflections between the stowed and the fully deployed flap cases, separate GVT test display models were created for configurations A and B. For configuration A, since there was little difference in the flap coordinate cases between the flap stowed and flaps slightly deployed, the same test display model was used for both cases. Figure 15 shows the test display models created for configuration A with the flaps stowed, slightly deployed, and fully deployed.

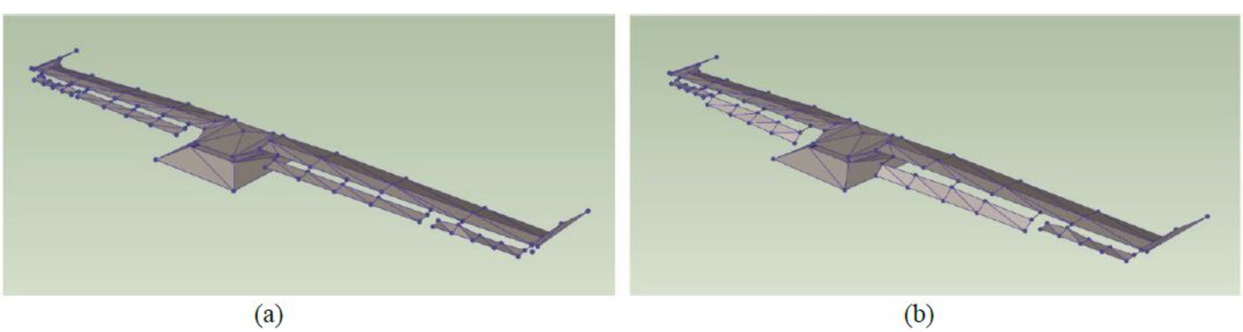

Fig. 15 Test display models or ground vibration test models for configuration A (Fig. 15a) with flaps stowed and flaps slightly deployed; and with flaps fully deployed configuration B (Fig. 15b)

Likewise, Fig. 16 shows the test display models created for configuration B, with the flaps stowed as well as the flaps fully deployed. The difference in configuration B versus configuration A is that the cruise nacelle mass simulator and wingtip plates were removed in the configuration B test display models.

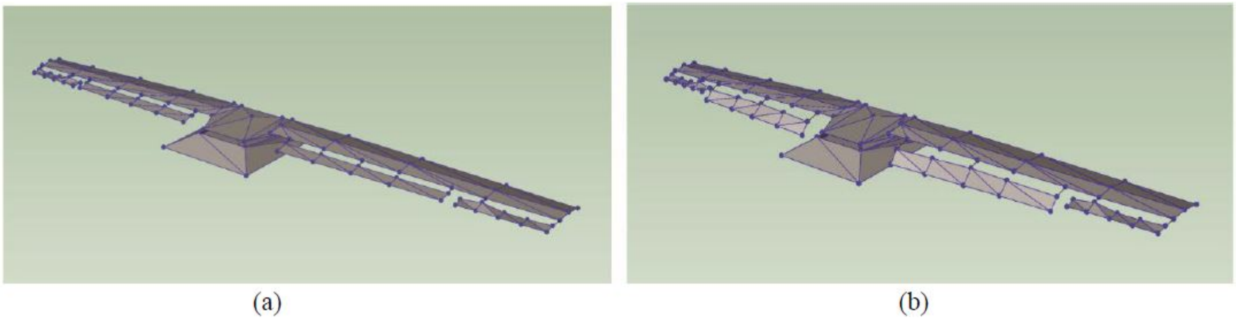

Fig. 16 Test display models or ground vibration test models for configuration B (Fig. 16a) with the flaps stowed; and the flaps fully deployed Configuration B (Fig. 16b)

Results

A total of 192 test runs were completed during the X-57 Mod III wing GVT. Data was gathered using BK Connect® software. The following sections discuss the modal test results for the two different wing configurations and at various flap settings, including configuration A with the flaps stowed, flaps fully deployed, and flaps slightly deployed, and configuration B with the flaps stowed and flaps fully deployed. With the flaps slightly deployed, configuration B was not performed as originally planned. Although GVT data was gathered for both ailerons in the locked, unlocked, and neutral position, only data from aileron locked cases is presented. Note that the FEM and GVT frequency comparisons, which are presented in the following sections, utilized the non-tuned FEM before correlation updates were performed.

Configuration A – Flaps Stowed

The Mod III GVT started with configuration A with the wingtip cruise nacelle mass simulators along with the flaps stowed and ailerons locked. Initial findings from this test configuration informed how the remainder of the GVT was to be conducted. There were several test runs that involved a four-shaker configuration with an additional two shakers (one at each of the left and right flaps); however, post-processing of those test runs indicated that the frequency response functions (FRFs) were not as clean as desired, and the four-shaker configuration was subsequently dropped for the remaining test runs. Normally, for shaker testing, burst random excitation is used. After the test conductors noticed that some of the accelerometers experienced a DC offset and that the time history decay in the data never settled out, the shaker excitation was switched to a continuous, random setting for the remainder of the test. In addition, impact hammer excitations were performed on the flaps and the ailerons to excite these control surfaces; however, post-processing of the impact hammer results during the GVT showed poor quality FRFs and mode shapes for the Mod III wing control surfaces. Data collected for the remainder of the test cases for configuration A exhibited similar results. As a result, the impact hammer excitation method was eliminated for the configuration B testing.

Table 5 lists the dominant wing and control surface modes with their GVT frequencies compared to FEM predictions for the Mod III wing in configuration A with the flaps stowed and ailerons locked. Mode names presented in Table 5 have been shortened to focus on the dominant motion. Percentage differences, highlighted in red, indicate that the error between GVT and the FEM frequency is greater than 5 percent. Frequency errors between the GVT and FEM predictions were consistently $>$5 percent starting at a GVT frequency of approximately 40Hz, which suggests coupling between WLTF and Mod III wing modes occurred at frequencies even lower than the 55 Hz (as predicted by the pre-test FEM of the Mod III wing mated to the WLTF). Visualization of mode shapes starting at approximately 40 Hz showed significant motion of the WLTF top plate (accelerometer node 9001-9004). This coupling between the WLTF and Mod III wing was observed in both configurations A and B.

Figure 17 shows the GVT mode shapes and frequencies for the dominant wing and the control surface modes that were listed in Table 5. What was noticed immediately was nearly all the modes exhibited asymmetry, with one side of either the wing or the control surface being more dominant than the other. Most of the wing modes were in line with the FEM predictions, with the exception of the anti-symmetric wing fore/aft (AWFA) and the symmetric wing fore/aft (SWFA) modes, as shown in Fig. 17c and Fig. 17d, respectively, which occurred at higher frequencies than expected. In addition, the AWFA and the SWFA modes were the only wing modes that showed no asymmetry between the left and right sides of the wing. The control surface modes with the flaps and ailerons also exhibited this asymmetry in their mode shapes, with the exception

Table 5 Configuration A – flaps stowed and ailerons locked: frequency comparison between finite element model and ground vibration test

Mode name	FEM frequency, Hz	GVT frequency, Hz	Percent difference from FEM	Notes on GVT mode shape
Anti-sym wing 1st bending (AW1B)	2.11	2.14	1.68%	Left wing dominant
Sym wing 1st bending (SW1B)	2.26	2.26	-0.05%	Left wing dominant
Anti-sym wing fore/aft (AWFA)	5.12	6.22	21.53%	Both wings dominant
Sym wing fore/aft (SWFA)	7.14	7.91	10.85%	Both wings dominant
Anti-sym wing 2nd bending (AW2B)	14.62	14.82	1.42%	Left wing dominant
Sym wing 2nd bending (SW2B)	15.62	15.76	0.89%	Right wing dominant
Anti-sym wing 1st torsion (AW1T)	21.89	22.81	4.21%	Left wing dominant
Sym wing 1st torsion (SW1T)	22.42	23.35	4.15%	Right wing dominant
Anti-sym flap sine wave bending	31.06	36.10	16.22%	Right-flap sine wave. GVT has no anti-sym shape. Only right flap responding.
Sym flap sine wave bending	31.12	40.89	31.42%	Left-flap sine wave. GVT has no sym shape. Only left flap responding.
Sym flap rotation	34.47	52.20	51.46%	Left-flap dominant
Anti-sym flap rotation	36.96	49.99	35.23%	Right-flap dominant with AWFA & right aileron bending
Anti-sym aileron rotation	46.21	100.11	116.66%	Left aileron dominant
Sym aileron rotation	46.93	122.79	161.67%	Both ailerons dominant
Anti-sym aileron bending	59.83	66.81	11.67%	Left aileron dominant
Sym aileron bending	61.41	68.43	11.43%	Right aileron dominant

symmetric (sym); anti-symmetric (anti-sym)

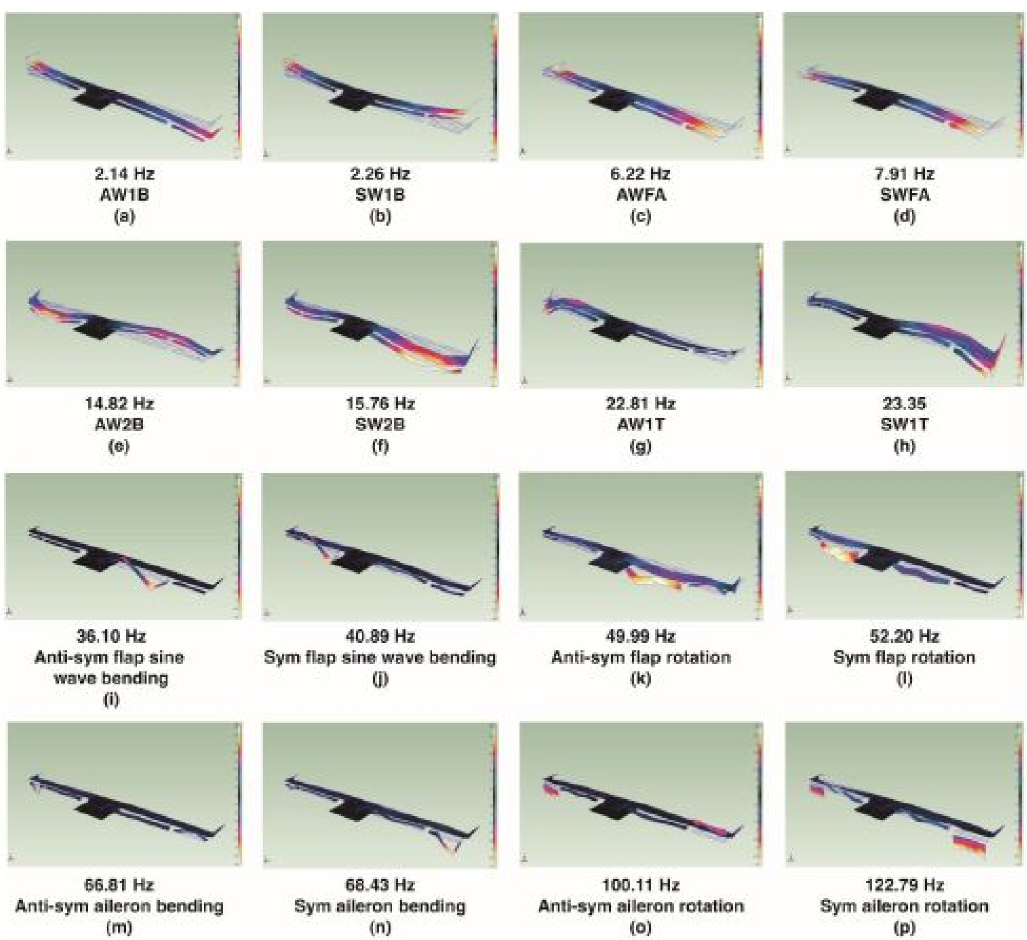

Fig. 17 Ground vibration test mode shapes and frequencies for configuration A – flaps stowed and ailerons locked

of the symmetric aileron rotation mode in Fig. 17(p). It should be noted that all GVT flap and aileron mode frequencies were much higher than what the FEM had predicted. Particularly, the anti-symmetric and symmetric aileron rotation modes exhibited well over a 100-percent frequency difference between the GVT and FEM, indicating that the aileron wing hinge and/or the GVT aileron actuation mechanism connection stiffness was more rigid than expected.

Configuration A – Flaps Deployed

For the next flap setting of configuration A, the flaps were deployed at the maximum deflection setting of approximately 30 degrees. This configuration checked for any significant effects to the mode shapes or frequencies, particularly for the flaps, when compared to the stowed-flap case. The GVT accelerometers on the flaps were releveled for orientation back into the aircraft coordinate system prior to the deployed flaps test runs since the flap accelerometers were initially installed when the flaps were stowed. Table 6 compares GVT frequencies between the wing and control surface modes of configuration A for the flaps stowed case in the left column, and the flaps deployed case in the right column. Percentage values in red indicate that the frequency shift between the flaps deployed case and the flaps-stowed case is greater than 5 percent magnitude. Note that pre-test FEM modal predictions were only done for both configuration A and B with the flaps stowed, so there were no direct GVT to FEM comparison for the cases where the flaps were either fully deployed or slightly deployed. Having the flaps fully deployed lowered frequencies for several flap modes compared to the flaps-stowed case. These modes included the right-flap sine wave bending, the left-flap sine wave bending, as well as the symmetric flap rotation mode. Although, the anti-symmetric flap rotation GVT mode frequency was lower than that of its counterpart in the flaps-stowed case, the difference was not as pronounced as the symmetric flap rotation mode, which was lower than the stowed GVT result by about 32 percent.

Table 6 Ground vibration test frequency comparison for configuration A between flaps stowed and ailerons locked versus flaps deployed and ailerons locked

Mode Name	Flaps stowed GVT frequency, Hz	Flaps deployed GVT frequency, Hz	% difference from flaps stowed
Anti-sym wing 1st bending (AW1B)	2.14	2.14	-0.15%
Sym wing 1st bending (SW1B)	2.26	2.26	0.03%
Anti-sym wing fore/aft (AWFA)	6.22	6.04	-2.95%
Sym wing fore/aft (SWFA)	7.91	7.54	-4.64%
Anti-sym wing 2nd bending (AW2B)	14.82	14.69	-0.89%
Sym wing 2nd bending (SW2B)	15.76	15.60	-0.96%
Anti-sym wing 1st torsion (AW1T)	22.81	22.84	0.14%
Sym wing 1st torsion (SW1T)	23.35	23.38	0.13%
Right-flap sine wave bending	36.10	30.59	-15.26%
Left-flap sine wave bending	40.89	32.58	-20.31%
Anti-sym flap rotation	49.99	47.50	-4.98%
Sym flap rotation	52.20	35.40	-32.18%
Anti-sym aileron bending	66.81	64.11	-4.05%
Sym aileron bending	68.43	68.90	0.69%
Anti-sym aileron rotation	100.11	96.96	-3.15%
Sym aileron rotation	122.79	115.27	-6.13%

Configuration A – Flaps Slightly Deployed

Configuration A with the flaps slightly deployed is similar to the flaps-stowed case with the following exception; when the flaps are released from their stops, a slight movement aft was created during flap positioning. In the case where flaps were slightly deployed, Table 7 shows a comparison of the GVT frequencies between the wing and control surface modes for configuration A with the flaps slightly deployed and the other two flap settings discussed earlier. The two right columns of the table show the percentage difference for the slightly deployed flap cases when compared to the stowed-flap and deployed-flap cases, respectively. Percentage values in red indicate frequency differences of greater than 5 percent. Wing modes did

Table 7 Configuration A – ground vibration test: frequency comparison between the flaps-stowed and flaps-deployed cases versus the flaps slightly deployed case

Mode name	Flaps stowed GVT frequency, Hz	Flaps deployed GVT frequency, Hz	Flaps slightly deployed GVT frequency, Hz	Percent difference from stowed	Percent difference from deployed
Anti-sym wing 1st bending (AW1B)	2.14	2.14	2.12	-1.26%	-1.11%
Sym wing 1st bending (SW1B)	2.26	2.26	2.23	-1.12%	-1.15%
Anti-sym wing fore/aft (AWFA)	6.22	6.04	6.11	-1.81%	1.17%
Sym wing fore/aft (SWFA)	7.91	7.54	7.54	-4.71%	-0.07%
Anti-sym wing 2nd bending (AW2B)	14.82	14.69	14.76	-0.45%	0.44%
Sym wing 2nd bending (SW2B)	15.76	15.60	15.76	0.04%	1.00%
Anti-sym wing 1st torsion (AW1T)	22.81	22.84	22.78	-0.12%	-0.25%
Sym wing 1st torsion (SW1T)	23.35	23.38	23.32	-0.11%	-0.23%
Right-flap sine wave vertical bending	36.10	30.59	30.56	-15.34%	-0.10%
Left-flap sine wave vertical bending	40.89	32.58	34.43	-15.80%	5.66%
Anti-sym flap rotation	49.99	47.50	N/A	N/A	N/A
Sym flap rotation	52.20	35.40	39.92	-23.53%	12.75%
Anti-sym aileron vertical bending	66.81	64.11	66.33	-0.72%	3.47%
Sym aileron vertical bending	68.43	68.90	67.23	-1.76%	-2.43%
Anti-sym aileron rotation	100.11	96.96	111.99	11.87%	15.51%
Sym aileron rotation	122.79	115.27	117.76	-4.10%	2.16%

not change much between the three different flap settings, less than 2 percent. Most of the significant change was seen in the control surface modes. Note that for this configuration (flaps slightly deployed) the anti-symmetric flap rotation mode was not found in the GVT. For the right- and left-flap sine wave vertical bending modes and flaps slightly deployed, the GVT frequencies were approximately 15 percent lower compared to the stowed-flap case. When compared to the deployed-flap case, the right-flap sine wave vertical bending was on par, whereas with the left-flap sine wave vertical bending, the slightly deployed flap case was slightly higher. The frequency difference between the slightly deployed flap case and the stowed case was also higher for the symmetric-flap rotation mode when compared to the deployed flap case; however, for the anti-symmetric aileron rotation mode (flaps slightly deployed), the GVT result was much higher for the deployed case as opposed to the stowed case.

Configuration B – Flaps Stowed

Configuration B represents the clean X-57 Mod III wing (i.e., the cruise nacelles mass simulator and its associated wingtip plates were removed prior to testing). Table 8 lists the dominant wing and control surface modes with their GVT frequencies, compared to the FEM for the Mod III wing in configuration B with the flaps stowed and ailerons locked. Mode names in Table 8 have been shortened to focus on the dominant motion. The FEM predictions presented are from the model using the fixed-wing boundary condition case without the WLTF incorporated. Percentage differences, highlighted in red, indicate that the error between GVT and FEM frequency is greater than 5 percent. Like the previous test configuration, configuration B saw coupling between the WLTF and the Mod III wing starting around a GVT frequency of approximately 40 Hz, which was lower than the 55 Hz predicted by the pre-test FEM.

Figure 18 shows the GVT mode shapes and frequencies for the wing and control surface modes listed in Table 8 for configuration B with the flaps stowed and ailerons locked. Similar to configuration A, many of the modes for both the wing and control surfaces exhibited asymmetry, with one side being more dominant than the other. As expected, removing the cruise nacelle mass simulators at the wingtips for the clean wing configuration increased the wing GVT frequencies. For the AWFA mode in Fig. 18(c), like in configuration A with the flaps stowed, the GVT frequency was higher when compared to the FEM; however, the GVT frequency for the SWFA mode in Fig. 18(d) was in line with what the FEM had predicted. Whereas both wings were equally dominant for the AWFA and SWFA modes for configuration A, with configuration B (with the flaps stowed), the asymmetry was seen again with the AWFA mode showing left-wing dominance and the SWFA mode showing right-wing dominance. In addition, both the anti-symmetric wing 1st bending (AW1B) and the symmetric wing 1st bending (SW1B) modes (shown in Fig. 18a and Fig. 18b, respectively), were about 8 percent lower than what the FEM had estimated. Unlike configuration A (flaps-stowed case), both the anti-symmetric wing 1st torsion (AW1T) and symmetric wing 1st torsion (SW1T) modes for this configuration were not exactly pure wing modes; the AW1T mode (shown

Table 8 Configuration B – flaps stowed and ailerons locked: Frequency comparison between finite element model and ground vibration test

Mode Name	FEM frequency, Hz	GVT frequency, Hz	Percent difference from FEM	Notes on GVT mode shape
Anti-sym wing 1st bending (AW1B)	6.32	5.76	-8.88%	Left wing dominant
Sym wing 1st bending (SW1B)	7.13	6.55	-8.21%	Right wing dominant
Anti-sym wing fore/aft (AWFA)	12.95	15.14	16.87%	Left wing dominant
Sym wing fore/aft (SWFA)	19.99	20.64	3.26%	Right wing dominant
Anti-sym wing 2nd bending (AW2B)	24.84	23.90	-3.78%	Left wing dominant
Sym wing 2nd bending (SW2B)	26.95	26.36	-2.20%	Right wing dominant
Anti-sym wing 1st torsion (AW1T)	N/A	84.43	N/A	NOT IN FEM: see Anti-sym aileron bending below.
Sym wing 1st torsion (SW1T)	N/A	51.15	N/A	NOT IN FEM: Left wing dominant with strong left-flap bending and left aileron bending
Anti-sym flap sine wave bending	31.09	41.61	33.86%	Left-flap sine wave. GVT has no anti-sym shape.
Sym flap sine wave bending	31.19	46.36	48.64%	Right-flap sine wave. GVT has no sym shape. Right-flap-outboard half dominant.
Sym flap rotation	35.65	N/A	N/A	DID NOT SHOW UP IN GVT
Anti-sym flap rotation	39.24	70.60	79.91%	Right-flap dominant with right aileron bending.
Anti-sym aileron rotation	46.42	89.28	92.32%	Both dominant with slight left wing torsion.
Sym aileron rotation	48.34	116.22	140.41%	Both dominant with slight left wing torsion.
Anti-sym aileron bending	58.66	84.43	43.93%	Left aileron dominant with anti-sym wing torsion (left dominant) & left-flap bending.
Sym aileron bending	58.82	78.71	33.81%	Left aileron dominant with sym wing torsion (left dominant) & left-flap bending.

symmetric (sym); anti-symmetric (anti-sym)

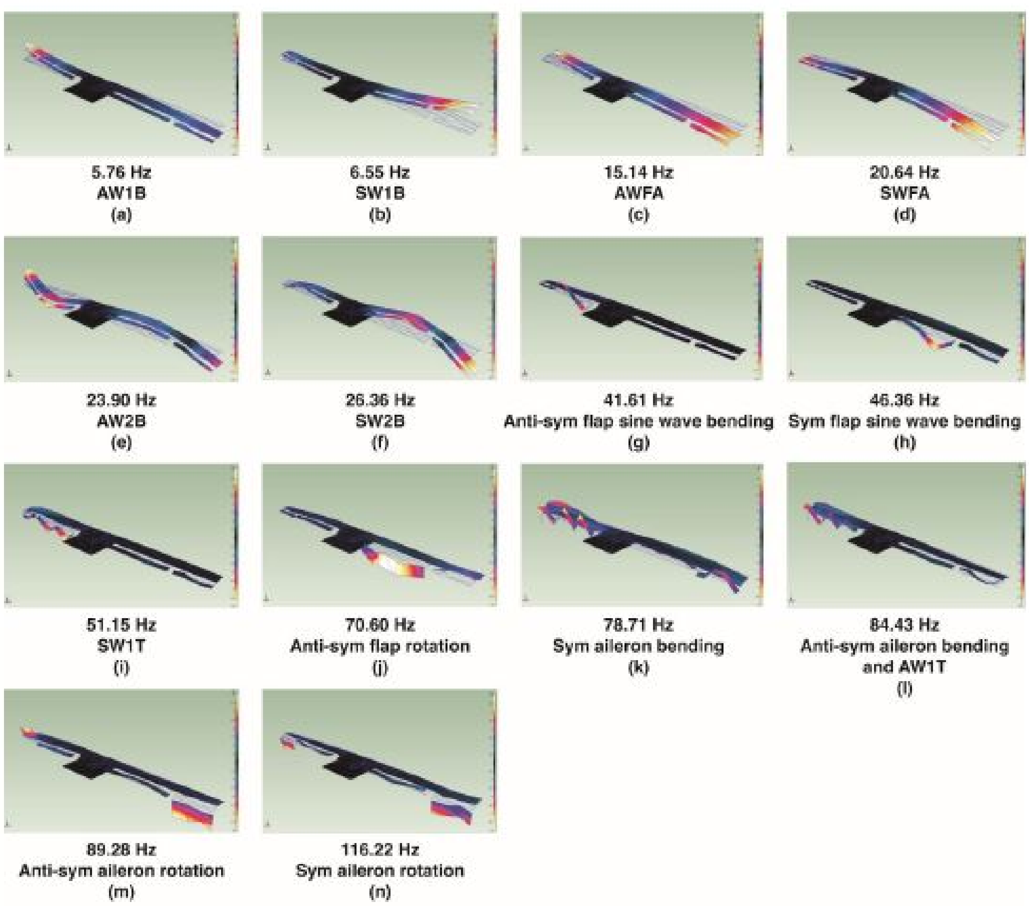

Fig. 18 Ground vibration test mode shapes and frequencies for configuration B – flaps stowed and ailerons locked

Table 9 Ground vibration test frequency comparison for configuration B between flaps stowed versus flaps deployed

Mode Name	Flaps stowed GVT frequency, Hz	Flaps deployed GVT frequency, Hz	Percent difference from stowed
Anti-sym wing 1st bending (AW1B)	5.76	5.83	1.21%
Sym wing 1st bending (SW1B)	6.55	6.69	2.15%
Anti-sym wing fore/aft (AWFA)	15.14	14.77	-2.42%
Sym wing fore/aft (SWFA)	20.64	18.57	-10.01%
Anti-sym wing 2nd bending (AW2B)	23.90	23.91	0.02%
Sym wing 2nd bending (SW2B)	26.36	25.80	-2.13%
Right-flap sine wave vertical bending	46.36	30.87	-33.42%
Left-flap sine wave vertical bending	41.61	32.57	-21.73%
Sym wing 1st torsion (SW1T)	51.15	57.68	12.77%
Sym aileron vertical bending	61.22	71.07	16.08%
Sym flap rotation	N/A	35.93	N/A
Anti-sym flap rotation	70.60	42.87	-39.28%
Anti-sym wing 1st torsion (AW1T)	84.43	56.54	-33.03%
Anti-sym aileron vertical bending	84.43	64.34	-23.79%
Anti-sym aileron rotation	89.28	92.10	3.16%
Sym aileron rotation	116.22	124.10	6.78%

in Fig. 18(l)) had some dominant-left aileron bending as well as left-flap bending, and the SW1T mode (shown in Fig. 18(i)) also exhibited similar behavior with the left aileron and the left flap. These results make sense since the wing torsion modes shift to much higher frequencies with the removal of the wingtip motor masses and illustrate how the wing was designed to support large motors mounted at the wingtip. It should be noted that the clean wing FEM did not predict the presence of either the AW1T or SW1T modes. For the flap and aileron modes, the GVT frequencies were significantly higher than the FEM predictions, similar to the flaps-stowed case for configuration A with the cruise nacelle mass simulators. Also, the symmetric flap rotation mode did not manifest during the GVT for this case.

Configuration B – Flaps Deployed

Table 9 lists the frequencies for the wing and the control surface modes for the case with the clean wing, where the flaps are deployed compared to the previous case with the flaps stowed. Percentage values in red indicate that the frequency difference between the two GVT results are greater than 5 percent magnitude. The only wing mode that had a large difference from the flaps-stowed case was the SWFA mode, which was about 10 percent lower. The remainder of the control surface modes saw big differences between the flaps-stowed and flaps-deployed cases except for both the anti-symmetric and symmetric aileron rotation modes. Having the flaps deployed probably reduced the stiffness and frequencies for the flap modes. Although the symmetric flap rotation mode did not appear in the clean wing case with the flaps stowed, it did show up when the flaps were deployed. For the anti-symmetric flap rotation mode, the dominant flap changed; for the flaps-stowed case, the right flap was dominant, whereas in the flaps-deployed case, the left flap was dominant. This complex modal behavior of the flaps in both configurations A and B suggest that the control surface exhibits some nonlinear behavior, which will be further discussed in the next section. In the clean wing flaps-stowed case, the AW1T and anti-symmetric aileron vertical bending modes were coupled, which resulted in a shared frequency, whereas in the deployed flap case, the modes were more independent of one another but still slightly coupled.

Flap Nonlinearity and Finite Element Model Correlation

From this ground vibration test, it was observed that the different flap deployment settings affected flap modal response for both frequency and damping. From the frequency response plot, shown in Fig. 19, the right- and left-flap modes showed shifts in frequency when compared to one another between the various flap settings, despite having the same excitation location and force level input for the three different test runs. Also, the damping values for the flap modes were four to eight times larger than those of the wing modes, possibly due to nonlinear joints, such as the spherical bearings, associated with the control surface actuation system.

For the FEM correlation, a reduced-order model was used to compare the analytical results to the GVT data. Most of the model tuning effort was focused on updating the joint properties as well as making sure the FEM matched the as-built hardware of the test article. NASA Technical Standard (NASA-STD-5002), Load Analyses of Spacecraft and Payloads, defines that for significant modes, agreement between test and analytical frequencies should be within a 5-percent margin, whereas off-diagonal terms of the cross-orthogonality matrix should be within 10 percent [8]. Note that correlation ofoff-diagonal terms of the cross-orthogonality matrix is usually difficult at higher frequencies, particularly for complex aerospace structures. Figures 20, 21, and 22 present cross-orthogonality comparisons before and after FEM correlation to the GVT data for the stowed, deployed, and slightly deployed flap settings for configuration A. The cross-orthogonality plots show fundamental wing modes and primary flap bending modes up to approximately 40 Hz and were well correlated but also highlight some limitations that were encountered. The Mod III wing GVT was performed on a fixture designed for the wing loads proof test. This test fixture had flexible modes starting at approximately 40 Hz, which affected the GVT-measured mode shapes. A FEM of the test stand was included during the FEM to GVT correlation; however, more accelerometer instrumentation measuring test stand modes were required, yet not available, to improve wing mode correlation $\geq$ 40 Hz. Another challenge noted was with regards to the FEM versus GVT difference, where no significant response corresponding to FEM modes 7 and 8 (flap modes) was measured during the GVT when flaps were stowed and slightly deployed (Figs. 20 and 22, respectively); however, these flap modes only showed up in the deployed case, as shown in Fig. 21. The flap modes were heavily damped in the test data and difficult to extract, likely resulting from the flaps being restrained by contact with the wing flap-cove surface while in the stowed position.

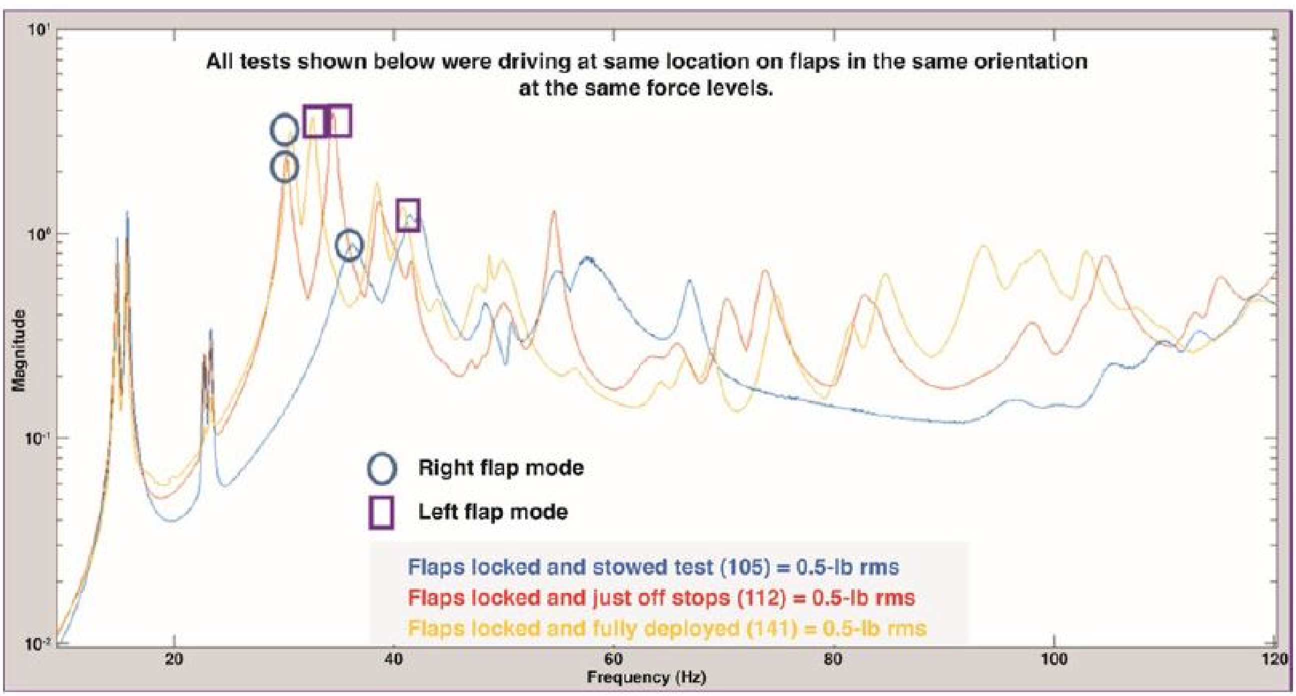

Fig. 19 Frequency response plot showing the nonlinearity behavior for the different flap settings for configuration A

FEM/Test Cross Orthogonality Table

FEM Shapes

			1	2	3	4	5	6	7	8	9	10	11	12	13	14	15	16	17	18	19
Otg	Test Shapes		2.17	2.35	4.62	7.37	15.11	16.32	19.07	19.27	22.74	23.54	31.87	33.10	33.17	38.02	41.60	42.24	45.99	47.87	48.86
100	1	2.13	100																	5	
95	2	2.25		100																	8
90	3	6.21			100																
85	4	7.88				100															
80	5	14.82	7				99				5									16	13
75	6	15.77		9				99				11									31
70	7	22.78					5	6			98	18								16	24
65	8	23.34				6		9			18	97								7	29
60	9	36.16												91	28			6		7	9
55	10	40.89	7							5			11	20	65		63	12	8	28	
50	11	41.35	9												18		75	52	9	42	6
45	12	42.30	7	9							5			10	19	9	55	65		6	47
40	13	44.26							23	7			10		18	89		21	7		11
35	14	48.30							7	6			60	5	7	5	9	6	67	42	19
30	15	52.32								8			40			26	6	5	68	42	12
25	16	54.77	5	7			6	6					8	6			7	10	5	40	17
20	17	57.21	5	6									5				22	16	10	22	
15	18	59.38	6	6			8	5					18				23	12	7	24	

Fig. 20a Cross-orthogonality matrix before correlation for configuration A – flaps stowed and ailerons locked

FEM/Test Cross Orthogonality Table

FEM Shapes

			1	2	3	4	5	6	7	8	9	10	11	12	13	14	15	16	17	18	19
Otg	Test Shapes		2.22	2.41	6.00	8.12	15.61	17.04	18.81	20.22	24.45	25.12	37.50	42.86	44.91	45.57	46.50	50.10	52.97	56.91	60.87
100	1	2.13	100	5																	
95	2	2.25		100																	
90	3	6.21			100																
85	4	7.88				100															
80	5	14.82	5				99	7													
75	6	15.77		7			6	99													
70	7	22.78									99	5									
65	8	23.34				6						99									
60	9	36.16											95			5	5			6	
55	10	40.89	6								5			36	87	20	13				
50	11	41.35	9										7	37	19	87	6				
45	12	42.30	6	8							5			25			91	11			6
40	13	44.26							17	13				80	10	27	40	23			
35	14	48.30								5				12		5	8	95	9		
30	15	52.32												7		8			94		27
25	16	54.77	5	6			6	5				6	7			7				91	
20	17	57.21		6															5	6	85
15	18	59.38	6	6			7				7										84

Fig. 20b Cross-orthogonality matrix after correlation for configuration A – flaps stowed and ailerons locked

FEM/Test Cross Orthogonality Table

Otg	Test Shapes		FEM Shapes 1 2.20	2 2.42	3 4.68	4 8.06	5 15.34	6 15.74	7 15.79	8 16.72	9 24.31	10 24.98	11 28.60	12 34.33	13 34.37	14 38.73	15 42.50	16 44.01	17 46.08	18 47.56	19 53.09
100	1	2.15	100																		
95	2	2.26	5	100																	
90	3	6.00			100																
85	4	7.52				100															
80	5	14.74					99	9	6												
75	6	15.63		7					9	99											
70	7	17.45						78	61	7			11								
65	8	19.63					9	63	76	10											
60	9	22.81									99						5				
55	10	23.37				5						99	12								
50	11	30.57											24	27	90						
45	12	32.58						5	5					92	27						
40	13	34.11						6				10	87		17			38		5	
35	14	38.43	6								5		15		5		92	20	13	13	5
30	15	40.79							5				32		5	20	40	78		9	
25	16	43.99	5		5								5			94	7	15		22	10
20	17	46.73	5					6					13				10	15	5	29	60
15	18	47.59									5		9			18			9	91	17
10	19	48.59	6		5						5					6	17	13		10	85
5	20	49.70	7							5	6					15	20			25	87
0	21	50.40		9			5					5	5					27			15
	22	56.34								6		5				13	15	13		16	17

Fig. 21a Cross-orthogonality matrix before correlation for configuration A – flaps deployed and ailerons locked

FEM/Test Cross Orthogonality Table

Otg	Test Shapes		FEM Shapes 1 2.23	2 2.43	3 6.01	4 8.14	5 15.44	6 16.84	7 17.29	8 18.33	9 24.44	10 25.16	11 34.36	12 34.49	13 39.35	14 42.37	15 43.56	16 45.52	17 49.55	18 53.72	19 54.77
100	1	2.15	100																		
95	2	2.26	6	100																	
90	3	6.00			100																
85	4	7.52				100															
80	5	14.74	5				100														
75	6	15.63		7				99	6												
70	7	17.45							99						9						
65	8	19.63								100											
60	9	22.81								5	99					6					
55	10	23.37				5						99									
50	11	30.57							6				96	12	5						
45	12	32.58								9			11	96							
40	13	34.11													96		10	13			7
35	14	38.43	6								5				12	65	68	18	6	5	
30	15	40.79							5						8	41	10	86			
25	16	43.99	5													70	61	14	32		
20	17	46.73	5						5						15	11		12	25	73	56
15	18	47.59									5					13	23	5	91	9	11
10	19	48.59	6		6						5					13	9	12	21	84	14
5	20	49.70	7					5			6					8	16	6	16	91	22
0	21	50.40		9			5					5			5			23			93
	22	56.34						7				6				5	13	9	15	14	12

Fig. 21b Cross-orthogonality matrix after correlation for configuration A – flaps deployed and ailerons locked

FEM/Test Cross Orthogonality Table

FEM Shapes

			1	2	3	4	5	6	7	8	9	10	11	12	13	14	15	16	17	18	19
Otg	Test Shapes		2.17	2.35	4.62	7.37	15.11	16.32	19.07	19.27	22.74	23.54	31.87	33.10	33.17	38.02	41.60	42.24	45.99	47.87	48.86
100	1	2.08	100	6																5	
95	2	2.24		100																	6
90	3	6.01			100																
85	4	7.51				100															
80	5	14.76	7				99				5									14	13
75	6	15.70		9				99				11									31
70	7	22.71					5	6			98	18								15	23
65	8	23.29				6		9			19	97								6	29
60	9	30.17							7				5	93	27						
55	10	34.43								9			13	26	85		25	14		12	14
50	11	38.54	5	5					5				36	6	5	5	45	74	20	52	27
45	12	39.93							9				82		7	29	31	25	15	7	10
40	13	41.54	9	6							6		11	8	26	8	76	41	10	23	37
35	14	44.51								7			24		10	94		10	7		
30	15	47.10		7					5	6		5	7			16	5	15	29	45	
25	16	48.30								15	7		5		12	15	5	17	91	63	27
20	17	49.14							5	15			26			21	25	8	78	57	12
15	18	49.89		7					5	10			14		5	7	7	17	46	6	14
10	19	50.32		5				5		12		5	8			24	17	17	70	58	10
5	20	54.50	7	7									5	7	24		15	8		17	15
0	21	63.11					5			13			14		11	8	6	7		5	
	22	65.65					13	7			15				6	6	7		10	9	17
	23	66.64		5			5	5			8	8	7								31
	24	70.14	7		6		18				5		6	6	5		10			23	23
	25	70.87		5				16		5				14							35

Fig. 22a Cross-orthogonality matrix before correlation for configuration A – flaps slightly deployed and ailerons locked

FEM/Test Cross Orthogonality Table

FEM Shapes

			1	2	3	4	5	6	7	8	9	10	11	12	13	14	15	16	17	18	19
Otg	Test Shapes		2.22	2.42	6.02	8.16	15.59	17.02	18.02	19.13	24.43	25.10	34.24	34.29	41.20	42.62	44.40	44.96	49.80	54.52	55.53
100	1	2.08	100	7																	
95	2	2.24		100																	
90	3	6.01			100																
85	4	7.51				100															
80	5	14.76	5				99	6													
75	6	15.70		7			6	99	6												
70	7	22.71									99	5				5					
65	8	23.29				5					5	99									
60	9	30.17							6				88	40	6						
55	10	34.43								9			37	82		8	22	14		9	5
50	11	38.54	5										5		36	38	38	70	11	6	6
45	12	39.93							6	5			7		86	12	33	31	14		
40	13	41.54	8	6							7		11	25	17	45	63	43		21	12
35	14	44.51								7				5	28	79	49		12		
30	15	47.10		6					6	5							10	23	30	56	68
25	16	48.30								16	7			11		7	14	20	89	12	
20	17	49.14								15					17	7	19	12	82	32	29
15	18	49.89		6						11					9			22	51	44	65
10	19	50.32						5		12		6					16	24	73	44	30
5	20	54.50	6	6									10	23			7			64	53

Fig. 22b Cross-orthogonality matrix after correlation for configuration A – flaps slightly deployed and ailerons locked

Summary

The X-57 Mod III wing ground vibration test was performed to gain a further understanding of the aeroelastic behavior of the Mod III wing structure. Two main configurations were investigated: the clean wing on its own, and a configuration that included the cruise nacelle mass simulators. For the most part, frequencies of the wing modes aligned well with finite element model predictions. Most of the error between the ground vibration test results and the finite element model predictions were for the flap and aileron modes and were significantly higher than anticipated, indicating the control surface modeling in the finite element model needed to be updated. Another problem in identifying and processing the ground vibration test results for these control surface modes was that these modes stay around or above the coupling frequency of the wing loads test fixture, which was lower than predicted. Using the fixed base correction method for this ground vibration test would have eliminated the coupling problem that was seen between the wing and the wing loads test fixture [9, 10]. Overall, the project gained some invaluable insight into the modal behavior of the Mod III wing, which contributed to the subsequent model updates to the Mod III wing finite element model as well as both the classical and whirl flutter analyses.

Acknowledgments The authors thank the X-57 project team and crew as well as the NASA AFRC FLL mechanics and technicians for assisting with the test setup and test execution of the X-57 Mod III wing GVT. The authors also thank Chris Moon and Doug Lovelace (from Hottinger Brüel & Kjær) for their assistance and support during the test. Finally, the authors thank the peer review committee, including Muhhamad Raza, Chan-gi Pak, and Benjamin Park, for taking the time to review this paper.

References

1. National Aeronautics and Space Administration, “X-57 Maxwell Overview,” X-57 Fact Sheet: https://www.nasa.gov/aeronautics/x-57-maxwell/ [accessed September 24, 2024].
2. Borer, Nicholas K., Geuther, Steven C., Litherland, Brandon L., and Kohlman, Lee, “Design and Performance of a Hybrid-Electric Fuel Cell Flight Demonstration Concept,” AIAA Paper 2018-3357, June 2018. doi: 10.2514/6.2018-3357
3. National Aeronautics and Space Administration, “Armstrong Flight Research Center,” https://www.nasa.gov/armstrong/ [accessed September 24, 2024].
4. National Aeronautics and Space Administration, “Flight Loads Laboratory Overview,” https://www.nasa.gov/flight-loads-laboratory-overview [accessed September 24, 2024].
5. National Aeronautics and Space Administration, “Flight Loads Laboratory,” Fact Sheet, https://www.nasa.gov/wp-content/uploads/2016/05/m187015fll_print_508.pdf [accessed September 24, 2024].
6. Miller, Eric J., Li, Wesley, Jordan, Ashante, and Lung, Shun-Fat., “X-57 Wing Structural Load Testing,” AIAA Paper 2020-3090, June 2020. doi: 10.2514/6.2020-3090
7. Bhamidipati, Keerti K., Pak, Chan-gi., Truax, Roger A., Winkel, James P., Rosario, Sev, Cutright, Stephen E., Massey, Steven J., and Wieseman, Carol D., ”Classical Flutter Analysis of X-57 Aircraft Mod II, III, and IV Configurations,” AIAA Paper 2024-4212. July 2024. doi: 10.2514/6.2024-4212
8. NASA Technical Standard, “Load Analyses of Spacecraft and Payloads,” NASA-STD-5002A, section 4.9.1, September 25, 2019.
9. Napolitano, Kevin L., and Yoder, Nathanael C., “Fixed Base FRF Using Boundary Measurements as References - Analytical Derivation,” Topics in Modal Analysis I, Volume 5, Proceedings of the 30th IMAC, A Conference on Structural Dynamics, Jacksonville, Florida, pp. 299-308, 2012. doi: 10.1007/978-1-4614-2425-3_27
10. Spivey, Natalie, Saltzman, Rachel, Wieseman, Carol, Napolitano, Kevin, and Smith, Benjamin., “Passive Aeroelastic Tailored Wing Modal Test Using the Fixed Base Correction Method,” Topics in Modal Analysis & Testing, Volume 8, Proceedings of the 38th IMAC, A Conference and Exposition on Structural Dynamics 2020,pp. 61-83, Houston, Texas, 2020. doi: 10.1007/978-3-030-47717-2_7